MECHANICAL PARAMETERS AND MATERIAL PROPERTIES, CONDITIONING ARREST OF AN UNSTABLE CRACK

H.C. van Elst*

It was envisaged to verify whether a specific material characterization can be given, governing arrest of an unstable fracture and not dependent on dimensions, geometry and applied load configuration. A critical s.i.f. at arrest, if providing for this, will still require fulfilling of validness conditions. Experiences with CLWL-specimens in the ASTM crack arrest co-operative program in this context are resumed, discussing required corrections.
Direct determination of the s.i.f. at arrest on Fe 510 steel proceeded from high speed photographic recordings of the isochromatics in a photo-elastic layer glued to a Robertson test steel plate and from straingauges recordings. The results were compared with the ASTM methodologies. It was concluded that straingauges recordings offer a convenient experimental way for finding the (dynamic) s.i.f. at arrest.
The c.d.f. at quasi static crack extension for fixed displacement was numerically evaluated for SENT-, CNT-, CT- and 3 points SENB-specimens.

INTRODUCTION

Arrest Capability Of A Structure As An Aspect Of Failure Control

Assuming time independent and only in a (small) interval varying material properties, further structural service circumstances (load and environmental endurances) only deviating from a certain (periodic) pattern in a restricted way as time proceeds, adequate design measures on mechanical grounds can meet, what can be called the necessary conditions for prevention of failure.

* TNO Division for Structural Engineering and Materials
P.O.Box 29 - 2600 AA Delft - The Netherlands

Ignoring departures from structural design in the construction a finite life time approximation can then be based on stochastic considerations for an assembly of similar structures under service by yet occurring violences of these two limited variation assumptions. Recognizing design departures like geometrical and (or) dimensional deviations, further flaws in the structural material as (initial) constructional realities, a deterministic life time assessment can be made. This follows from the convergence in time of an increasing subcritical deviation under the service circumstances in an assumedly known way and its possibly decreasing critical value by material degradation under the service endurances or by intrinsic material developments, also assumedly known. For the critical value of a deviation, instability will result or anyway loss of fitness for purpose. This is e.g. demonstrated for a (flat) flaw by its characterizing increasing subcritical s.i.f., eventually attaining its possibly decreased critical value. This causes unstable fracture- or such a flaw might earlier have obtained a critical (time independent) value in structural sense, as penetration of wall thickness of a vessel, leading to "leak before break", preventing further service operation. It is also demonstrated by an initially present deflection having a subcritical value for buckling and increasing e.g. by creep to a critical valuě for this (possibly again decreased by material deterioration in time).
This stated insight in deviations tolerance implies which eliminations, as by repair of initial subcritical design departures, have to be made in order to meet ambitions for a certain service time. It obviously firstly requires detection of such "faults" by non destructive techniques. Overlooking of some of these cannot be excluded and a full guarantee for absence of failure during service, i.e. indications of the sufficient conditions for this, can thus not be given. While during construction plastic deformation ("setting"), welding, etc. might already cause initial flaws and material degradation, apart from the material delivery condition showing faults, moreover non tolerable faults might be generated, as service time proceeds. In particular extreme variances in load and environmental endurance, e.g. rises in temperature gradient ("hot spots") not foreseen in the design, caused by accidental loss of service control or due to external influences (as earth quake, earth slide, flooding, (air) traffic accident, military or terroristic actions etc.) - if not already leading to immediate failure - can lead to local or global material damage. This can further promote initiation of faults - also of those hitherto considered as acceptable ("sleeping") and a decrease of critical value, resulting in failure.
Recommended periodic non destructive inspection can reveal previously unnoticed and newly generated defects, - also local or global material damage (to which often insufficient inspection attention is paid!) - to be judged on further acceptance. Periodically corrected life time assessments can thus be made.

At the end of the envisaged service life a remaining life time estimate can be given (the latter preferably in combination with destructive testing methods).
Before tackling stochastic life time assessments, bearing on the above mentioned aspects, and further based on distribution functions of relevant material properties and endurances (either experimentally determined or just guessed) the arresting capability of the structure for a possibly generated unstable fracture can be taken into account. This will be based on possibly present design measures for such arrest (like "arresting holes", stiffeners, temperature gradients causing a fracture to run into hotter, i.e. tougher material, insertion of tougher material parts etc.) and on the global, possibly in time degrading, material properties, providing for this. If possible a differentiation of arrest capability as to material properties and design aspects thus appears useful.
At present there still appears to be lack of consensus regarding the existence of such a material property, e.g. the s.i.f. at arrest, viz. whether this is not dependent on geometry and (or) dimensions or load. Presumably an influence of (plastic) constraint ("thickness") will anyhow remain, like for the s.i.f. at initiation. If an arrest characterizing material property like the s.i.f. at arrest exists, the establishment of an order of merit for structural materials as to this, appears a most useful rubrication.

Objective And Scope Of This Investigation

It was envisaged trying to verify, whether the toughness at arrest as indicated by the s.i.f. or J-integral, noted by K_{Im} or J_{Im} resp. is an unambiguous material parameter - and if this is confirmed - to develop a convenient experimental way for its determination. In view of this, participation in the activity mentioned next appeared appropriate.

Co-operative Program On Crack Arrest Toughness Measurement

This was recently performed under auspices of ASTM E24.03.04. The existence of an unambiguous K_{Im} was accepted and the possible influence of kinetic energy generated by the unstable fracture on the arresting conditions investigated. MRL and BCL took the initiative for this program.
CLWL-specimens of two types (Figures 1a and 1b) were set available to participants in different countries. The s.i.f. at arrest, according to MRL and BCL prescriptions, given in the appendices to the prospectus on the program (1), were determined in order to verify, which methodology might offer the best reproduceable s.i.f. at arrest. In these approaches BCL takes the kinetic energy into account, K_{Im} in their view being the minimum of the crack velocity dependent s.i.f., K_{Id}, at arrest.

MRL uses a quasi static approach in which the s.i.f. at arrest, K_{Ia} rather functions as K_{Im}. The theoretical background for both approaches was well documented ((1), (2a), (2b), (3)) and will not be discussed here.
The results of the performed ASTM round robin arrest program (ARRAP) were reviewed and discussed by BCL and MRL in (4). Before elaborating on here further performed arrest experiments with (a practical off-shore) Fe510 steel, to possibly establish the existence of K_{Im} and convenient ways to find it, it appears appropriate to resume our experiences with the ARRAP (on which individual reports did not appear in open literature to our knowledge). This allows to indicate what required corrections in our opinion have to be added to the prospectus prescriptions, which were hinted at in the summary of (4), but not specifically detailed.

The Crack Arrest Investigation On Fe510 Steel

Direct determinations of the s.i.f. at arrest from high speed photographic recordings of the dynamic isochromatics, using a photo-elastic layer glued to the test plate, and from straingauges recordings, were carried out in the Robertson test.
For K_{Ia} and K_{Id}, recordings, according to MRL and BCL respectively, the crack initiation of CLWL-specimens proved to require much lower test temperatures than the RCAT and a comparison with the s.i.f. from dynamic recordings was not directly possible. This was due to the photo-elastic material prematurely loosening from the steelplate at the applied lower test temperatures for CLWL-specimens - and the straingauges having similar difficulties. However from the assumed temperature dependence of the s.i.f. or rather c.d.f. at arrest, which was related to that of Charpy-V impact values as discussed, a comparison yet seemed possible. These results as well as those obtained in the ARRAP (also as here reported) confirmed the statement in the ARRAP summary of (4), that no significant preference for K_{Ia} or K_{Id} could be given (the remaining basic problem being the debated existence of K_{Im})

EXPERIMENTS AND RESULTS

Procedures And Applied Corrections In The ARRAP

Initiation of fast running cracks was achieved by displacement controlled transverse loading of CLWL-specimens (cf. Figures 1a and 1b). Recordings in time of wedge load, loadline displacement, or displacement at or near notch opening, proceeded with the aid of a fast (Kaman) displacement transducer.
From the displacement values at initiation and arrest (theoretical) values of the (plane strain) crack arrest toughness were deter-

mined. Guidelines for test performance and subsequent calculations are given by BCL and MRL in (1).
Six CLWL-specimens provided by MRL (Figure 1a),
two prepared from AISI 1018 steel and four from A533B steel, all subjected to a prescribed amount of precompression along the specimen load line, shortly prior to testing for favoring initiation and four CLWL-specimens provided by BCL (Figure 1b),
set at disposal as duplex specimens, consisting out of two parts, joined together by electron beam welding (fusion line detection transversal to anticipated crack, crack starter section from AISI 4340 steel, arrest section from A533 steel) were investigated. These were tested on fracture arrest, using a Kaman displacement transducer. The specimens had a thickness of 50.8 mm and were side grooved to 0.75 x thickness (for details of dimensions and geometry, cf. Figures 1a and 1b). A 250 kN loading capacity (Schenck) machine was used with the specimens horizontally positioned. Loading of the wedge, inserted between split pins, mounted in the specimenhole, proceeded with 0.1 mm/sec speed.
Of the MRL-specimens two from AISI 1018 steel and two from A533 B steel were tested at 20°C; two from A533 B steel were also tested at 0°C.
Of the BCL-specimens two from A533 B steel were tested at 20°C and two from A533 B steel were tested at 0°C (crack starter section AISI 4340 steel).
For the experiments at 0°C the specimens were placed in a metal box and immersed in a (cooling) liquid; temperature control was by thermocouples. Displacement controlled loading continued till the "run and arrest" event had taken place. After arrest "heat tinting" and then complete separation by loading in liquid nitrogen (77°C) was performed. The length of the initial notch and the arrested crack were measured and the calculations prescribed by BCL and MRL carried out. The presence of non connected crack areas behind the crackfront at arrest could be micrographically demonstrated. Examples of recordings in time of wedge load and notch opening displacement (9 mm from the specimen edge) and of wedge load versus load displacement are shown in Figures 2a and 2b for a MRL- and BCL-specimen resp.
The wedge load and displacement values at crack initiation and arrest were deduced from these recordings.
The results, using the by MRL and BCL proposed calculation procedure (cf. relevant reference curves in (1)) are given in TABLE 1, together with the occurring crack jump $a-a_o=\Delta a$ and other connected data. K_Q is the s.i.f. providing for initiation.
As a result of further analysis given below, it became clear, that still substantial corrections to the s.i.f. evaluations were neceassary, which are elaborated next.

The corrections to the MRL-and BCL-procedure for fracture toughness evaluation at arrest.

According to (1) (cf. also "Numerical and analytical analysis...." below): K_Q and K_{Ia} were found for the MRL-specimens from:

$$K(\lambda) = (E/\sqrt{W}).(B/B_N)^{\frac{1}{2}}\ Y(\lambda)\Delta \quad \ldots\ldots\ldots\ldots\ldots\ldots\ldots\ldots (1)$$

1> B/B_N = thickness ratio of possibly applied side grooving
Δ = displacement of crack edges at 0.25 W from loadline.
W = width; λ = a/W; $Y(\lambda)$ is given by MRL in (1), app.A sub 9. 1.8.

K_Q and K_{Ia} were found for the BCL-specimens from:

$$K(\lambda) = (E/\sqrt{W}),(B/B_N)^{\frac{1}{2}}.\chi(\lambda)v \quad \ldots\ldots\ldots\ldots\ldots\ldots\ldots\ldots (2)$$

v = displacement of crack edges in load line.
$\chi(\lambda)$ is given by BCL in (1), app. B. Table 3.

The geometrical correction factors of the s.i.f. for CT-specimens with constant H/W and λ=a/W>0.35 are equal, irrespective of D/H with 2H=specimen height; 2D=distance between centres of pinholes; cf. Tada's handbook of s.i.f. (5).
This conclusion still holds, when the pinholes distance 2D approaches zero, i.e. for the wedge loaded specimens. Also the diameters of the pinholes up to values well above those for the MRL-type specimens (0.15 W) or for the BCL-type specimens (0.25 W) have negligeable influence on this observation. Consequently the BCL-reference curve for determination of K_{Id} from K_{Id}/K_Q and λ was used for the MRL-type specimens as well, measuring v. For the evaluation procedure, according to MRL was used: $Y(\lambda)=H(\lambda)(v/\Delta)/EBC=\chi(\lambda).v/\Delta$ with $H(\lambda)$, v/Δ and C dependent on λ.
According to (1), data of H, v/Δ and C for a CT-specimen have been used, whereas CLWL-specimens were tested in the MRL-procedure. Though $H(\lambda)$ and C for a CT- and CLWL-specimen remain practically equal and unchanged in a wide range of λ=a/W values (cf. the above quoted results of Tada (5)), the values of v/Δ for these specimen types for corresponding λ=a/W are different for λ<0.7.
Consequently the $Y(\lambda)$ functions for both specimen types differ also. This is illustrated in Figure 3, using calculations of Newman (5). The data according to Crosley and Ripling (1), (7) to evaluate $Y(\lambda)$ are shown as well. Thus the $Y(\lambda)$-values from (1) have been corrected by multiplying $Y(\lambda)$ with $(v/\Delta)_{CLWL}/(v/\Delta)_{CT}$, taking the required (v/Δ)-values from (6); corrected K-values for MRL-type specimens are indicated as K* in TABLE 1.

TABLE 1 - $\underline{K}_{Ia}$ and $\underline{K}_{Id}$ evaluations from Crack Arrest Testing in ARRAP with CLWL-test specimens of:

A) MRL-type

Specimen codenr.	material steeltype	temp. (°C)	a_o (mm)	a_o/W	Δ_i (mm)	Y_i	K_Q (MPaVm)	K_Q^* (MPaVm)	K_Q^{**} (MPaVM)	Δa (mm)	$\Delta a/W$	Δ_a (mm)	Y_a	K_{Ia} (MPaVm)	K_{Ia}^* (MPaVm)	K_{Ia}^{**}	K_{Id} (MPaVm)	K_{Id}^* MPaVM)	K_{1d}^{**}
6341/02	AISI 1018	20	59.0	0.35	1.09	0.214	135	172		44.8	0.263	1.13	0.155	101	108		105	134	
6341/43	AISI 1018	20	58.8	0.35	1.04	0.214	129	164		50.0	0.293	1.09	0.147	93	98		98	125	
106A	A533B	20	59.1	0.35	1.38^5	0.214	171	218		58.0	0.340	1.43^5	0.135	112	117		124	158	
406A	A533B	20	59.3	0.35	1.07	0.214	132	168		46.6	0.275	1.10^5	0.151^5	96.5	103		102	130	
503A	A533B	0	58.9	0.35	1.08	0.214	133	170		51.4	0.301	1.13	0.145	94.5	100		100	128	
110B	A533B	0	59.0	0.35	1.22	0.214	151	192		65.2	0.384	1.28	0.124	91.5	94		106	134	

*values obtained by multiplying uncorrected K-values with $(v/\Delta)_{CLWL}/(v/\Delta)_{CT}$ for relevant λ.

b) BCL-type

					v_i (mm)							v_a (mm)								
RG 134	A533B	20	68.8	0.33	1.09	0.351	200	183	184	53.8	0.258	1.13	0.218	129	119	130	166	152	152
RD 40	A533B	20	68.8	0.33	1.30	0.351	239	217	218	28.9	0.139	1.32^5	0.273	190	172	178	F	F	F
RG 128	A533B	0	69.3	0.33	1.19	0.351	220	205	192	99.3	0.481	1.21	0.127	81	75.5	75.5	141	133	124
RG 132	A533B	0	68.6	0.33	1.18	0.531	218	209	199	82.0	0.393	1.21	0.166	106	102	94.5	152	147	140

* values obtained from corrected v, by extrapolation of (Δ, v)-recording to Δ=0.

** values obtained from Δ at 0.212 W = 44 mm from loadline.

F outside BCL-reference diagram; fracture arrested in weld.

However another correction still proves required as well. For the BCL-type specimens not only the loadline displacements v, but also edge displacements Δ' at 0.212W from the loadline were measured, while for the MRL-type specimens not only the edge displacements Δ at 0,25 W, but also load line displacements v' were measured. This was performed with an XY-recorder, plotting v ' vs. $\Delta^{(')}$. While the advanced part of these recordings showed a linear relationship the part near the origin was curved, the relative increase of v ' being larger than $\Delta^{(')}$. This was attributed to a setting of the splitpins and a possibly additional deformation of the flanges of these splitpins (in fact the displacement between these flanges was measured and taken as load line). In order to correct for this last mentioned effect, the straight part of the recording of v ' vs.$\Delta^{(')}$ was extrapolated and the intersection with v ' =0 taken as corrected origin. K-values for BCL-type specimens were accordingly corrected with v measured with respect to this latter origin: In this way corrected s.i.f. are listed as K* for BCL-type specimens in TABLE 1.
K-values for the BCL-type specimens were also calculated from Δ'. As these were measured at 0.212W from the loadline (instead of 0.25W, as with the MRL-type specimens) an interpolation procedure was applied, based on data from Newman (6). Thus obtained further corrected s.i.f. values are indicated as K** for BCL-type specimens in TABLE 1.
The uncorrected and corrected s.i.f. values were plotted versus relative crackjumplength in Figure 4a and 4b for 20°C and 0°C resp. The applied corrections reduce previously present differences between the results in MRL- and BCL-specimens resp. and between K_{Ia} and K_{Id} themselves.
The differences in K_Q, the s.i.f. at initiation, will be due to the introduction of residual stresses (as by the welding of the BCL-dual specimens) and by the variations in notch preparation (including the precompressing). If K_Q is higher, Δa is larger and K_{Ia} is smaller.
It is further recalled that from the displacement recordings at initiation and immediately after the crackjump, using the l.e.f.m. compliance data, the load and thus the s.i.f. is evaluated. As after the crackjump the load relaxes, the compliance rather refers to the physical cracklength and so does K_{Ia}.
This might imply an underestimate as a plastic zone size correction for the physical crack, accounting for the relevant notional crack length, appears appropriate.
At loading up to initiation the compliance will refer to the notional crack and underestimates of K_Q can be present as well. (Prescriptions in (1) try to compensate for this, but still imply uncertainties in our opinion.) This can be of importance for K_{Id} evaluations according to BCL for which the correct indication of K_Q is essential; cf. (1).

Characterization of Investigated Fe510 Steel

This steel was chosen as test material, as it is widely applied in practice, a.o. in off-shore structures. It was delivered as 12.5, 25 and 50 mm thickness plate in quantities of 6 m^2, 18 m^2 and 6 m^2 resp., rolled from the same cast.
Characterizing material properties are given in TABLES 2, 3 and 4, while Figures 5a, 5b, 5c, and 5d, show the Charpy V-transition curves.

TABLE 2 - Chemical Composition of investigated Fe510 steel

Si	C	Mn	P	S	Cu	Cr	W	Al	Nb	Mo
0.46	0.15	1.41	0.013	0.012	0.03	0.02	0.02	0.02	0.02	0.0004

TABLE 3 - Mechanical Properties of investigated Fe510-steel

thickness (mm)	yield point (MPa)	UTS (MPa)	elongation (%)
12.5	390	526	38.3
25.0	391	541	31.2
50.0	361	513	29.0

TABLE 4 - Isothermal Crack Arrest Temperatures in Robertson tests (RCAT) of investigated Fe510 steel

thickness (mm)	specimen dimensions LxW in mmxmm	applied gross stress (MPa)	RCAT (°C)
12.5	300x320	235	-30 to -33
25.0	300x320	235	-16 to -20
50.0	300x320	215	0 to - 5

The RCAT's were determined by using a 4000 kN Robertson test loading machine. Specimens (as shown in Figure 7) were inserted into this machine and loaded to nominal stress levels 60% of the yield stress. A temperature gradient was then established by suitably local cooling and heating devices. An unstable fast running crack was initiated by firing a steel pin from a boltgun against the nose of the specimen, cooled with liquid nitrogen. Crack initiation from the root of a small sawcut at the circumference of a hole drilled in the specimen nose, is then ascertained. Five thermocouples rather equally spaced along the anticipated crack path at the specimen surface allow temperature control. The temperature at the tip of the arrested crack in

temperature gradient tests could thus be found by interpolation. Isothermal tests were subsequently performed by cooling specimens to an uniform temperature, as monitored by the previous test result, indicating the arrest temperature in a gradient test (which is higher than the isothermal crack arrest temperature). At and above the arrest temperature in isothermal Robertson tests, the initiated unstable fracture stops; below this arrest temperature the specimen is totally severed.

Initiation Techniques and Estimates of K_{Ia} and K_{Id} for Fe510 Steel

12.5 and 25 mm thick Fe510 steel CLWL-specimens of the MRL-type were prepared, be it without side grooves.
In order to facilitate crack initiation, deformation and subsequent ageing of a 18 mm diameter zone near the notch root was performed. A knife was pressed in the material at the notch root, providing for a rather sharp initial notch.
Four straingauges were glued on the specimen along the anticipated crackpath. At the arrest test a uniform temperature was maintained in the ligament; the notch root required no extra cooling for initiation.
Load and crack edge displacement were recorded both versus load line displacement and as a function of time, using transient recorders, which also served to store the straingauges signals. The transient recorders were triggered by a fifth straingauge bonded at the embrittled initiation zone.
Required test temperatures for initiation proved considerably below the RCAT. K_{Ia} and K_{Id} evaluations were performed, applying necessary corrections, as elaborated above; relevant data are given in TABLE 5a.
K_Q-values for Fe510 steel were invalid, even taking into account the relevant increased yield strength of the deformation aged initiation region. As only l.e.f.m. compliance considerations for the K_{Id} assessments from the BCL-reference curves in (1) come into play, some uncertainty results in their indication.
The experimental v/Δ values for the Fe510 steel arrest investigation are in between Newman's results for the CLWL-and CT-specimens; they are higher than those resulting from Crosley and Riplings's work.

Recording of the Dynamic Isochromatics in Photo-elastic Material Glued to a Plate of Fe510 Steel experiencing an (Arresting) Unstable Fracture, Offering a Dynamic S.I.F. Estimate (at Arrest)

A Cordin model 470 framing camera was at disposal for a few tests. Framing speed could be varied between 2×10^5 and 2×10^6 f.p.s.; total number of frames was 80; frame picture dimensions 18x24 mm; time between successive frames in a series of 80 pictures can thus be varied between 0.5 and 5 μs, corresponding

TABLE 5 - K_{Ia} and K_{Id} evaluations for Fe510 steel:

a) from CLWL-MRL type specimen testing (cf. fig. 1a), according to MRL and BCL procedures resp.:

CLWL-MRL specimen codenr.	thickness (mm)	temp. (°C)	a_o (mm)	a_o/W	Δ_i (mm)	Y_i	K_Q (MPaVm)	K_Q* (MPaVm)	Δa (mm)	$\Delta a/W$	Δ_a (mm)	Y_a	K_{Ia} (MPaVm)	K_{Ia}* (MPaVm)	K_{Id} (MPaVm)	K_{Id}* (MPaVm)
31	12.5	-58	69	0.41	1-38	0.202	140	168	86	0.50	1.41	0.065	46	46	88	105
32	12.5	-42	72	0.42	0.81	0.200	85	101	12	0.07	0.75	0.184	69	78	80	95
34	12.5	-50	75	0.44	1.18	0.196	116	136	21	0.12	1.20	0.167	101	111	103	121
35	12.5	-60	72	0.42	1.14	0.200	114	136	26	0.16	1.16	0.162	94	102	99	118
30	25	-60	59	0.35	1.33	0.214	143	182	92	0.54	1.35	0.073	49	49	86	109
33	25	-58	60	0.35	1.48	0.214	159	203	n.a.	-	-	-	-	-	-	-
36	25	-59	69	0.41	0.96	0.202	97	117	27	0.15	0.94	0.167	79	87	83	100

N.B. 1. K*-values obtained by multiplying uncorrected K-values by $(v/\Delta)_{CLWL}/(v/\Delta)_{CT}$ for relevant a/W.
2. Applied low temperature allowed static initiation from locally aged cracktip.
3. n.a. = no arrest.

b) from Robertson type specimen testing (cf. fig. 7a), using h.s.p.; initiation by impact + local cooling.
K_{Ia} from f.e.m. calculations; K_{Id} from recorded dynamic isochromatics.

Robertson specimen codenr.	thickness (mm)	temp. (°C)	a_o (mm)	length (mm)	width (mm)	σ_o (MPaVm)	a_a (mm)	K_{Ia} before arrest	K_{Ia} after arrest	K_{Id} before arrest	K_{Id} after arrest
60	12.5	-15	-	300	320	215	160	33		139	
64	25	-10	-	1000	320	210	185	161		132	
59	25	-10	-	300	320	210	185	83		137	
?	25	-20	-	300	320	210	n.a.	-		106	
53	50	- 2	-	300	320	210	n.a.	-		105	

c) from Robertson type specimen testing (cf. fig. 7c), using straingauges; initiation by impact + local cooling
K_{Ia} from (6d); $K_{Id} = K_{Ia}\sqrt{1-V/c_R}$

								p (mm)	V (ms^{-1})				
22	50	-10	-	300	320	215	n.a.	12.5	410	122		115	
23	50	- 5	-	300	320	215	n.a.	26.0	430	152		143	
24	50	0	-	300	320	215		14.0	430	146	84	137	79

d) from SENT type specimen testing (cf. fig. 8), using straingauges; static initiation
K_{Ia} from (6d); $K_{Id} = K_{Ia}\sqrt{1-V/c_R}$.

SENT specimen codenr.													
25	25	-19	45	160	200	187		12.5	414	110	69	103	65
29	25	-19	45	160	200	194		12.5	443	117	63	110	59

with a total camera recording time between 40 and 400 μs resp. The frequency of the rotating mirror, a triangular reflecting prism, could be read on a counter display, offering the camera recording time. Colourfilm (Ectachrome) 400 ASA was used in all tests. The light source was a Cordin model 607. The deviation of its (approximate) rectangular time performance could be chosen between 40 and 625 μs; usually 300 μs was used.
Six measuring channels of transient recorders were available. One was used for measurement of the light flash duration and intensity; the second was used for recording of the trigger pulse; the remaing four measured the output signals of strain-gauges along the anticipated crack path, as elaborated below.
The s.i.f. at arrest in Fe510 steelplate specimens at the Robertson test was estimated from recordings of the dynamic isochromatics in photo-elastic material, glued at both sides of the anticipated crack path on the steelplate by filming with the aid of the above described h.s.p. equipment before, at and after arrest. For a number of tests the "run and arrest" phenomena was caught by the camera in the envisaged way. At analysis of the developed films the debonding of the photo-elastic material near the crack path, where the deformation is largest, proved to have occurred more rigorously than previously assumed. No isochromatics in the vicinity of the crack path could thus be analyzed. However close to the crackpath the plastic region will anyhow distort the elastic isochromatics response and interpretations of observations in that region appear difficult and were here rejected beforehand (this appears inherent to other ways of deformation recordings quite near the cracktrip as well, though the non-elastic responding region will be smaller than statically estimated). The debonding of the photo-elastic material also prevented indication of the exact crack tip location. This again is less problematic than might be thought at first glance, as at the analysis of the results for estimating the s.i.f. at arrest a notional crack has to be introduced with length equal to the sum of physical crack length and a part (50%) of the dynamic plastic zone size, the isochromatics actually defining this notional crack tip by their shape. Outside the non-elastically responding crack tip region the relatively simple Sneddon formula can be used, though at larger distances the Westergaard stress description, be it for finite dimensions, has to be applied, moreover in a dynamic sense for the here considered case. Regretfully only one or two isochromatics as colour fringes could be observed in this region, the more remote isochromatics running out of the viewing field of the camera.
As the intensity of the available (white) light source proved to be hardly sufficient for these tests, the prescribed diapositive film with a sensitivity of 400 ASA had to be developed according to 1600 or even 3200 ASA. Consequently the colours on the film were rather pale and the isochromatics rather vague.
From the static description of the stresses, according to the Westergaard analysis for a centrally cracked infinite plate in the

elastic case, the polar equation of the isochromatics with respect to the crack tip were resumed; cf. (8). The reduced static isochromatics, i.e. those for crack size 1, for uniaxial loading of an inifinite plate were plotted on transparencies for (integer) values of the parameter n with: $\sigma_1-\sigma_2=2n\tau_o=2nf\sigma_o$ (n = fringe number; $f\sigma_o=\tau_o$ = shear stress corresponding with unit fringe difference). It proved rather satisfactory possible to achieve coincidence of one of the calculated reduced static Westergaard isochromatics (for an infinite plate with a central crack under uniaxial load transversal to the crack) and a suitably magnified photograph of an isochromatic of certain colour recorded in the Robertson test. The s.i.f. values of the calculated reduced static Westergaard isochromatic, analytically known, was then taken equal to that of the dynamic isochromatic. This was considered a suitable, less time consuming method than fitting the dynamic isochromatic by an analytical description from which K could be deduced; cf. e.g. Rossmanith and Irwin (9). Thus evaluated s.i.f. at arrest are presented in TABLE 5b. An example of recorded isochromatics is shown in Figure 6.

Dynamic Recordings with Straingauges of Stress Performance during Crack Propagation and Arrest in Fe510 Steel and their Interpretation

Typically four straingauges were attached to "Robertson test" specimens for which fracture occurred by impact in order to check the applied stress and to record at crack propagation the inherent time variation of local stress as well as its velocity, cf. Figures 7a, 7b and 8 .
In particular the local stress variations for specimens in which the crack arrested and for those in which the crack runs through were compared. The dynamic s.i.f. was estimated from these recordings as elaborated below.
The straingauges were located at 12.5 mm from the anticipated crack path, consecutive straingauges were at different sides of this. Their mutual distance was 50 or 65 mm; the first straingauge was at 155 or 105 mm from the saw cut root. The output of the straingauges was stored in transient recorders and plotted afterwards.
Triggering was realized by an electrical contact in the hole of the (Robertson) specimen nose, which was closed at impact, causing initiation. The possible influence of the applied impact (for initiation at the Robertson test) on the response of straingauges (glued along the anticipated crack path) could be made negligeably small after suitable adaptations and modifications of the electrical circuit.
Several topographies for the bonding of 4 to 5 straingauges have been applied. Typical straingauges responses at performance of Robertson tests with specimens prepared as detailed in Figures 7a and 7b are shown in Figures 9a, 9b and 9c.

Responses of straingauges from SENT-specimens (cf. Figure 8) which were statically initiated, are shown in Figures 9d and 9e. The peak strain of a straingauge reflecting the passage of the crack front, corresponds to strain values, leading to stresses notably higher than the static yield strength. However at the moment of crack passage the dynamic yield strength appears relevant and the momentaneous recording will allow an elastic estimate of K_I^d, providing dynamic yield is not reached. Indeed the strain rate sensitivity of steel Fe510 is presumably such high, that at the straingauge location yield still appears absent on the moment of crack passage.

From a static evaluation of the s.i.f. (according to the goniometric Snedden approximation near the crack tip of Westergaard's description) and applying a dynamic correction factor $\sqrt{1-V/c_R}$ with $c_R = 0.92\sqrt{\mu/\rho}$ = Rayleigh velocity $\sim 3850\ ms^{-1}$; V = fracture velocity ν = Poisson's ratio = 0.28, the dynamic s.i.f. was estimated; cf. (10) in which a simplified solution of considerations of Freund (11) in this respect is given.

A justification of this approach based on the retardation of the near cracktip stress field adjustment, due to the finite Rayleigh velocity c_R can be given as follows:

Using the static approximation for mode I of the crack tip stress field:

$$\sigma_x = \frac{K}{\sqrt{2\pi r}} \cos\frac{\theta}{2}\left(1 - \sin\frac{\theta}{2}\sin\frac{3\theta}{2}\right) - \sigma_o \quad \ldots\ldots\ldots\ldots\ldots\ldots (3a)$$

$$\sigma_y = \frac{K}{\sqrt{2\pi r}} \cos\frac{\theta}{2}\left(1 + \sin\frac{\theta}{2}\sin\frac{3\theta}{2}\right) \quad \ldots\ldots\ldots\ldots\ldots\ldots (3b)$$

(r and θ, radius and polar angle resp. with respect to crack tip),

one can indicate the angle θ for which the response of a straingauge at distance p from the assumedly straight crack path to be realized, shows a peak.

The straingauge measures a deformation

$$E\varepsilon_y = \sigma_y - \nu\sigma_x = \frac{K}{\sqrt{2\pi p}} F(\theta) + \nu\sigma_o \quad \ldots\ldots\ldots\ldots\ldots\ldots (4a)$$

$$F(\theta) = \sqrt{\sin\theta}\left\{\cos\frac{\theta}{2}(1-\nu) + (1+\nu)\sin\frac{\theta}{2}\sin\frac{3\theta}{2}\right\} \quad \ldots\ldots (4b)$$

at quasi static interpretation according to the mentioned Irwin-Sneddon approximation of the Westergaard solution for stress description near the crack tip. For $\nu = 0.28$ a maximum will be shown for $\theta = 69°.7$ and $\{F(\theta)\}_{max} = 1.13$.

For p = 0.0125 m; $E = 2.1\times10^5\ MNm^{-2}$ and $\varepsilon_o \equiv \sigma_o/E \sim (2/3)\,\sigma_Y/E$

$K^s = (\varepsilon_{ymax} - \nu\varepsilon_o)\ E\ \sqrt{2\pi p}/\{F(\theta)\}_{max}$
$= (\varepsilon_{ymax} - 0.28\varepsilon_o) \times 51607\ MNm^{-3/2}$.

(The response of the straingauge at the time of passage of the crack tip appeared for the p-value elastic, due to the dynamic effect implying a high strain rate, though afterwards the relaxation of the elastic strain might turn into plastic deformation.)

For a crack velocity V the near crack tip stress field at a (surface) point P with momentaneous polar radius r and polar angle θ with respect to the crack tip O will show a retardation of its adjustment in the sense that it will be governed by the crack tip position O_o at which P had polar radius r_o and polar angle θ_o.
In the time $t = r_o/c_R$, that signals from θ_o, running with velocity c_R, reach P, the crack tip moves from O_o to O over a distance $V.r_o/c_R$. From the relevant geometry one concludes:

$$r \sin\theta = r_o \sin\theta_o = p = y_P \quad \ldots\ldots\ldots\ldots\ldots\ldots\ldots\ldots \text{(5a)}$$

$$r^2 = r_o^2 + (Vr_o/c_R)^2 - 2r_o(Vr_o/c_R)\cos\theta_o$$
$$= r_o^2(1+\beta^2) - 2r_o^2\beta\cos\theta_o \text{ with } \beta \equiv V/c_R \quad \ldots\ldots\ldots \text{(5b)}$$

$$r^2/r_o^2 = \sin^2\theta_o/\sin^2\theta = 1+\beta^2-2\beta\cos\theta_o$$

$$(\text{or } \cos^2\theta = (\beta\cos\theta_o)^2/(1+\beta^2-2\beta\cos\theta_o) \quad \ldots\ldots\ldots\ldots\ldots\ldots \text{(5c)}$$

As a consequence the assumedly present stress singularity term in the near crack tip stress field with $r^{-\frac{1}{2}}$, which has as (θ and r independent) coefficient K^d, will imply:

$$\sigma_y = \frac{K^d}{\sqrt{2\pi r}}\ f(\theta) + \ldots = \frac{K^d}{\sqrt{2\pi p}}\ \sqrt{\sin\theta}\ f(\theta) + \ldots = \frac{K^s\sqrt{\sin\theta_o}}{\sqrt{2\pi p}}\ f(\theta_o) + \ldots \quad \ldots\ldots \text{(6a)}$$

$$K^d = K^s\sqrt{\sin\theta_o/\sin\theta}\ f(\theta_o)/f(\theta) = K^s(1+\beta^2-2\beta\cos\theta_o)^{\frac{1}{4}}\ f(\theta_o)/f(\theta) \quad \ldots\ldots\ldots\ldots \text{(6b)}$$

$$K^d = K^s(1-\beta)^{\frac{1}{2}}\left\{1 + \frac{2\beta}{(1-\beta)^2}(1-\cos\theta_o)\right\}^{\frac{1}{4}} f(\theta_o)/f(\theta) \quad \ldots\ldots\ldots \text{(6c)}$$

In the plane of the crack where crack extension assumedly takes place θ and $\theta_o \to 0$, implying:

$$K^d = K^s(1-\beta)^{\frac{1}{2}} \lim_{\theta_o \to 0}\left\{1 + \frac{2\beta}{(1-\beta)^2}(1-\cos\theta_o)\right\}^{\frac{1}{4}} f(\theta_o)/f(\theta)$$

$$K^{d} = K^{s}(1-\beta)^{\frac{1}{2}} \quad \ldots\ldots\ldots\ldots\ldots\ldots\ldots\ldots\ldots\ldots\ldots\ldots \quad (6d)$$

$$[(\text{as } \lim_{\theta \to o} f(\theta) = \lim_{\theta_o \to o} f(\theta_o) \ (=1)]$$

For $\nu=0.28$; $\theta_{o,m} = 69°.7$ (for which the maximum response of the straingauge with distance p from the crack path occurred) and e.g. $\beta=1/7$ one finds $\theta_m = 77°.72$ and $K^d = K^s.0.98$ ($\cos\theta_{o,m}=0.3469$; $\sin\theta_{o,m}=0.9379$; $\cos\theta_m=0.2126$; $\sin\theta_m=0.9771$)
The s.i.f. results of straingauges recordings for relevant data as shown in Figures 9a, 9b, 9c, 9d, and 9e are assembled in TABLE 5c and 5d for 50 mm thick Robertson test specimens and 25 mm SENT-specimens, resp.

DISCUSSION

The Arrest (or Near Arrest) S.I.F. Values for Fe510 Steel, According to Different Methods and Diffferent Specimen Geometries

These are resumed in TABLE 5.
In order to find out, whether K_{Id} or K_{Ia} values possibly deserve preference as material parameter, characterizing fracture arrest, the consistency of obtained values for these with respect to temperature change and specimen change was analyzed. As elaborated before, direct comparison of different geometries and methods for one temperature regretfully proved difficult here, in view of the required initiation temperature at the MRL- or BCL-procedures being much lower than the RCAT for Fe510 steel. Although a priori knowledge on the temperature dependence of K_{Ia} or K_{Id} is not available - and this also was lacking for K_{Ic} - the Sailors-Corten-suggestion was accepted, which relates Charpy-V impact values to K_{Ic}, according to: $K_{Ic} = 15.5\ (CVN)^{\frac{1}{2}}$; cf. (12).
This offers: at -60°C: $K_{Ic} = 77.5$ MPaVm; at -10°C: $K_{Ic} = 109.6$ MPaVm. For the impact value of transversally taken Charpy-V-specimen (as relevant here) rises from 25 to 50 Joules, when increasing the temperature from -60°C to -10°C, as illustrated in Figure 5a (presumably G_{Ic} is thus doubled).
Assuming that in an appreciable suitable temperature interval between the lower and upper shelf levels the temperature curves of G_{Im}- and Ch.V-values are also parallel, a comparison of s.i.f. values at different temperatures can be made. For 25 mm thickness Fe510 steel the K_{Id} value 137 MPaVm for (or near) arrest from recordings of dynamic isochromatics in the Robertson test (TABLE 5b; specimen 59: lengthxwidth = 300 x 320 mm) at -10°C and the K_{Id} value 109 MPaVm for arrest at -60°C in CLWL-specimen testing, according to the BCL-procedure (cf. TABLE 5b, specimen 30) show rather good correspondence with the temperature dependence, as predicted from the Sailors-Corten relation. However the K_{Ia}-value 83 MPaVm for arrest at -10°C in the

Robertson test (TABLE 5b, specimen 60 lengthxwidth = 300 mmx320 mm) estimated using relevant f.e.m. calculations on which is elaborated below, and the K_{Ia}-value 49-87 MPaVm for arrest at -60°C in CLWL-specimen testing according to the MRL-procedure for the same 25 mm thickness Fe510 steel (TABLE 5a; specimen 30 and 36) do not allow to conclude to less compatibility with respect to temperature change, in view of the rather large inaccuracies in the K_{Ia}-determinations. For besides the scatter in CLWL-specimen testing results, it has to be noted that the K_{Ia}-values for the 300 mm length Robertson specimen, using the f.e.m. calculations, appear doubtful. A plateau level for the c.d.f. in the Robertson test, as suggested by the irreproducibility of the arrested crack lengths is gratifyingly confirmed by f.e.m. calculations for the quasi-static case, pertaining to the assumedly relevant situation of fixed rigid edges displacement. This is shown in Figure 10a; cf. also (8). However for specimen length 300 mm this plateau c.d.f. level is much lower than corresponds with the dynamic s.i.f. from the observed isochromatics. For with $K_{Ia} \sim K_{Id}/\sqrt{1-V/c_R}$ (see above) one would expect $K_{Ia} \sim 137\sqrt{1-462/3850} = 146$ MPaVm.

For relevant λ=0.78 the f.e.m. calculations offer:

$$kK_{Ia}^2 = EG_{Ia} = \sigma_o^2 WG^{**}(\lambda) = 215^2 \times 0,32 \times 0,48 = 7100 \text{ MNm}^{-1} \rightarrow K_{Ia} = 84.3 \text{MPaVm}$$

G^{**}, explained below (cf. (8b), increases with L (considering σ_o and W constant). For L=300 mm length is G^{**}=0.48 and for L=1000 mm length is G^{**}=1.64 (cf. Figure10a), which would imply for:

K_{Ia}=146 MPaVm and thus $G^{**} = K_{Ia}^2/\sigma_o^2 W = 146^2/215^2 \times 0.32 = 1.44$

$$L_{eff} = \left\{ \frac{1000-300}{1.64-0.48} \times (1.44-0.48 + 300 \right\} \text{mm} = 879 \text{ mm}$$

This would require an effective length much larger than the nominal length to be accounted for by the grips assembly, which appears difficult to understand.

Though rotations connected with a presumably present pin loading might occur, which can have an increasing effect on G^{**} and thus on K_{Ia}, these are expected to proceed mostly after arrest. Their influence will anyhow be insufficient to raise K_{Ia} to the level of ~ 146 MPaVm.

As a quite soft loading machine was used load relaxation by crack extension for fixed (translational) displacement will not occur accroding to $dP/da = -P/C\ dC/da$, but according to:

$dP/da = (-P\ dC/da + \Delta L_M)/(C+C_M)$

This results rather in an increase of σ than L, compared to σ as calculated by f.e.m. with the specimen loaded in an infinite stiff machine and at quasi static crack extension.

In Figures 10b, 10c, and 10d, the c.d.f. at quasi static crack extension for fixed displacement for a CNT-, CT- and SENB-specimen according to f.e.m. calculations is shown.

The most important reason for σ being larger than estimated from load relaxation of quasi static crack extension, appears to be the occurrence of reflection of the unloading stress waves at the specimen sides. These add to the tension at the crack tip in a periodic way causing K_I^d to be substantially larger than K_I^a. This strikingly confirms the base of the BCL-approach and do would imply K_{Ia} and K_{Id} evaluations being clearly at variance in principle.
Note in further accordance that the straingauges recordings both on 50 mm thick Robertson specimens (lengthxwidth = 300 mmx320 mm) and on SENT-specimens (lengthxwidth = 160 mmx200 mm) offered from quasi static interpretation of near crack tip observations K_{Ia}-values in accordance with the dynamic isochromatic recordings (TABLE 5b, 5c, and 5d).
It illustrates that real K_{Ia}-values are rather equivalent to K_{Id}-values for arrest characterization, as in fact suggested by the relation $K_{Id} \sim K_{Ia}\sqrt{1-V/c_R}$ if $V/c_R \ll 1$
However K_{Ia}-evaluations according to quasi static numerical analysis might require large corrections (in the dynamic case). A reliable and simple K_{Ia}, K_{Id}-evaluation appears the experimental one performed with straingauges, as elaborated above.

Consequences of Required Initiation Methods for Crack Arrest Toughness Evaluation According to MRL and BCL-Procedure

The K_{Id}-values for Fe510 steel from CLWL-specimen testing will be influenced by the applied deformation ageing required for initiation. It is expected that the prediction of K_{Ic}-values according to Sailors-Corten from Charpy V-values for the aged material, would be better compatible with determined K_Q values and resulting K_{Id} than of the material "as-is".
Yet at the here relevant temperature of -60°C this hardly comes into play as one is then dealing with the lower shelf level. Compressive residual stresses as introduced by the punch loading for the ageing procedure, will have been relieved by the heat treatment and applied precompression in the length direction. Still present compressive stresses would cause an increase in K_Q; their presence is corroborated by the K_{Ic}-values of the aged material, as predicted from the Sailors-Corten relation, being lower than K_Q.
The inaccuracy in the K_Q-values due to remaining internal stresses attributed to variations in notch preparation quite unfavorably interferes with K_{Id}-estimates and has to be considered a most disturbing factor.
A great difficulty to apply the MRL- or BCL-experimental procedure to a practical steel of interest like the here investigated Fe510 steel, thus proves the realization of initiation of an unstable fracture in absence of residual stresses. Static initiation in Fe510 steel could only be achieved by combination of deformation ageing and considerable temperature decrease.

Influence of Load and Dimensions on Arrest Temperature and Temperature Dependence of Arrest Fracture Toughness

Usually the arrest temperature only slightly increases with increasing σ_o for $\sigma_o > 2/3\sigma_Y$ and more clearly increases for $\sigma_o < 2/3\ \sigma_Y$. Increase of dimensions for constant σ_o (e.g. $2/3\ \sigma_Y$) only slightly increases the arrest temperature.
This suggests that in a rather small temperature interval around the arrest temperature, as determined for a Robertson test specimen (lengthxwidth = 300 mmx320 mm) and an applied gross stress $\sigma_o = 2/3\ \sigma_Y$, the fracture toughness will steeply rise with increase of temperature. The RCAT can be looked upon as the "transition temperature" of the dynamic fracture toughness.
Its obvious present upper shelf level can be approached by increasing c.d.f. as at increase of σ_o, though this is limited by the yield strength and (or) at increase of L, though this is limited by a L/W-ratio of the order 4. Above this ratio the static c.d.f. rather equals that for a strip with infinite length and can be analytically approximated, using the asymptotic K-solutions, as given in (13). (However a ductile unstable fracture above the RCAT by sufficiently large values of L and σ_o, appears a priori possible for accomodating fracture toughness behaviour.)
From the dynamic point of view a limiting length $L_c = W\ c/\dot{a}$ will exist, which implies for $\dot{a}$ = 0.4-1 mm/µsec a limiting length of 5 W to 12.5 W.

Numerical and Analytical Analysis of the Influence of Geometry and Dimensions on the C.D.F. at Quasi Static Crack Extension under Fixed Displacement Conditions for SENT-, CNT-, CT- and SENB-Specimens

F.e.m. calculations of G (λ) for fixed displacement were carried out by evaluation of C (λ), using a c.d.f. description according to:

$$G = \frac{P^2}{2B}\frac{dC}{da} = \frac{P^2}{2BW}\frac{dC}{d\lambda} = \frac{P_o^{\,2}}{BW}\frac{C_o^{\,2}}{C^2}\,\tfrac{1}{2}\,\frac{dC}{d\lambda} = \frac{\sigma_o^2 W}{E}\left(\frac{C_o^{\,*}}{C^*}\right)^2 \tfrac{1}{2}\,\frac{dC^*}{d\lambda} \equiv$$

$$\frac{\sigma_o^2 W}{E}\,G(\lambda)^{**} = E\varepsilon_o^2 W G(\lambda)^{**} \qquad \text{.....(8a)}$$

with $C^* = EBC$; $G^{**}(\lambda) = \left(\frac{C_o^{\,*}}{C^*}\right)^2 \tfrac{1}{2}\,\frac{dC^*}{d\lambda}$; .....(8b)

N.B. $K = \frac{\sigma_o\sqrt{W}}{k}\sqrt{G^{**}(\lambda)}$; G^{**} = c.d.f. for $\sigma_o^2 W/E = 1$

(k = 1 for plane stress; $k = 1-\nu^2$ for plane strain)
An analytical description of c.d.f. for fixed displacement offers:

$$G = \frac{P^2}{2B}\frac{dC}{da} = \frac{\sigma^2 WB}{2}\frac{dC}{d\lambda} = \frac{kK^2}{E} = \frac{k\sigma^2 W\lambda F(\lambda,\omega)^2}{E} \quad \ldots (9a)$$

with $K = \sigma\sqrt{W}\sqrt{\lambda}F(\lambda,\omega)$; $\omega \equiv W/L$

$$\frac{dC}{d\lambda} = \frac{2k}{EB}\lambda F(\lambda,\omega)^2 \equiv \frac{2k}{EB}\Phi(\lambda,\omega) \quad \ldots\ldots\ldots\ldots\ldots (9b)$$

$$C = \frac{2k}{EB}\int_0^{\lambda}\Phi(\underline{\lambda},\omega)d\underline{\lambda} + C_o = \frac{2k\Psi(\lambda,\omega)}{EB} + \frac{L}{EBW}$$

$$= C_o(2k\omega\Psi+1) \quad \ldots\ldots\ldots\ldots\ldots\ldots\ldots\ldots\ldots\ldots (9c)$$

$$\sigma = \sigma_o/(2k\omega\Psi+1) \quad \ldots\ldots\ldots\ldots\ldots\ldots\ldots\ldots\ldots\ldots (9d)$$

Fixed displacement $\Delta L = C_o P_o = CP$:

$$\Delta L = \frac{\sigma}{E}(2kW\Psi+L); \quad \varepsilon_o = \frac{\Delta L}{L} = \frac{\sigma_o}{E} = \varepsilon(2k\omega\Psi+1) \quad \ldots (9e)$$

$$G = \frac{(\Delta L)^2}{2BWC^2}\frac{dC}{d\lambda} = \frac{(\Delta L)^2}{2BWC_o^2}\frac{2k\Phi/EB}{(2k\omega\Psi+1)^2}$$

$$= E\varepsilon_o^2 W\frac{k\Phi}{(2k\omega\Psi+1)^2} = \frac{\sigma_o^2 W}{E}\cdot\frac{k\Phi}{(2k\omega\Psi+1)^2} \rightarrow$$

$$G^{**}(\lambda,\omega) = \frac{k\Phi(\lambda,\omega)}{\{2k\omega\Psi(\lambda,\omega)+1\}^2}$$

THEORETICAL REMARKS

Following Bui {(14), (15)} one can distinguish between intensity factors at the crack tip with respect to stress and with respect to (normal) crack opening displacement discontinuity. It appears appropriate to indicate the former now as dynamic (K^{σ}) and the latter as kinematic (K^{u}). The current literature indication of "dynamic" s.i.f. (K^{d}) - also followed here in the foregoing -then corresponds with $K^{\sigma}(t)$.
This applies to fracture modes I, II, and III.
While in the (quasi) static case for a crack with constant length 2a (and moving with constant velocity V) $K^{\sigma}=K^{u}$, one has in the arbitrary transient case {(14), (15)}:

$$K_I^u/K_I^\sigma = \frac{4}{\kappa+1}\,\frac{\alpha_d(1-\alpha_s^2)}{4\alpha_s\alpha_d-(1+\alpha_s^2)^2} \quad \ldots\ldots\ldots\ldots\ldots\ldots\ldots \quad (10a)$$

with $\kappa = 3-4\nu$ for plane strain and $\kappa = (3-\nu)/(1+\nu)$ for plane stress and $\alpha_d^2 = 1-V^2/c_d^2$; $c_d^2 = (\Lambda+2\mu)/\rho$; $\alpha_s^2 = 1-V^2/c_s^2$; $c_s^2 = \mu/\rho$; c_d = velocity dilatational waves; c_s = velocity shear waves; ρ = density. Note that with $\nu=\Lambda/2(\Lambda+\mu)$ one has $4/(\kappa+1)= 1/(1-\nu)=2(\Lambda+\mu)/(\Lambda+2\mu)$ in plane strain and $4/(\kappa+1)=1/(1+\nu)= (2\Lambda+\mu)/(3\Lambda+2\mu)$ in plane stress.
K_I^u/K_I^σ varies from 1 for V=0, to infinite for $4\alpha_s\,\alpha_d-(1+\alpha_s^2)^2=0$, i.e. $V=c_R$.
In the static case one has for the displacement of crack edges at distance x_o behind the cracktip (15):

$$[u_2(x_o)] = u_2(x_o, \pi) - u_2(x_o, -\pi) = K_I^u\,\frac{\kappa+1}{\mu}\,\left(\frac{x_o}{2\pi}\right)^{\frac{1}{2}} \text{ with}$$

$$K_I^u = K_I^\sigma = K_I^s = K_I$$

From retardation considerations in view of the finiteness of c_R, similar to those leading to (6a) one alternatively concludes for the dynamic case: $K_I^u(t)\{x(t)\}^{\frac{1}{2}} = K_I(x_o)^{\frac{1}{2}}$ and thus with $x(t) = x_o + Vt = x_o + x_o\,V/c_R$, one has $K_I^u(t) = K_I(1+\beta)^{-\frac{1}{2}}$ and

$$K_I^u/K_I^\sigma = (1-\beta^2)^{-\frac{1}{2}} \quad \ldots\ldots\ldots\ldots\ldots\ldots\ldots\ldots\ldots\ldots\ldots\ldots (10b)$$

Current considerations for introducing the J-integral, but now for the non-equilibrium situation, i.e. $\sigma_{ij,j}=\rho u_{i,tt}$, read:

$$w = \int_o^{\varepsilon_{ij}} \sigma_{ij}\,d\varepsilon_{ij};\quad w_{,k} = \sigma_{ij}\,\varepsilon_{ij,k} = \sigma_{ij}u_{i,jk} = (\sigma_{ij}u_{i,k})_{,j} - \sigma_{ij,j}u_{i,k}$$

$$= (\sigma_{ij}u_{i,k})_{,j} - \rho u_{i,tt}u_{i,k}; \quad \ldots\ldots\ldots (11a)$$

$$\rho u_{i,tt}u_{i,k} = \rho(u_{i,t}u_{i,k})_{,t} - \rho u_{i,t}u_{i,kt} = \rho(u_{i,t}u_{i,k})_{,t} - \tfrac{1}{2}\rho(u_{i,t}u_{i,t})_{,k};$$

$$w_{,k} - (\sigma_{ij}u_{i,k})_{,j} + \rho(u_{i,t}u_{i,k})_{,t} - \tfrac{1}{2}\rho(u_{i,t}u_{i,t})_{,k} = 0 \quad \ldots\ldots\ldots (11b)$$

$$\{(w-\tfrac{1}{2}\rho u_{i,t}u_{i,t})\delta_{kj} - \sigma_{ij}u_{i,k}\}_{,j} + \rho(u_{i,t}u_{i,k})_{,t} = 0 \quad \ldots\ldots\ldots (11c)$$

{conservation law of Fletcher (16)}

For k=1 and steady state crack extension with velocity V:

$$J^d = \int_\Gamma (wn_1 - \sigma_{ij}u_{i,1}n_j - \tfrac{1}{2}\rho u_{i,t}u_{i,t}n_1)ds + \delta/\delta t \int_A \rho u_{i,t}u_{i,1}dA$$

$$- \int_{\partial A} \rho u_{i,t}u_{i,1}Vn_1 ds \quad \ldots\ldots\ldots\ldots\ldots\ldots\ldots\ldots\ldots (12)$$

Γ is a contour moving along with the crack of length 2a, connecting two points (P_u and P_d) on opposite crack edges by going around the crack tip; it encloses a surface A of which the border ∂A comprises Γ and two straight crack border surfaces from P_u and P_d towards the crack tip, plus a vanishing circle around this crack tip; cf. (15).

$$\text{N.B. } \frac{\delta}{\delta t}\int_A f dA \equiv \int_A \frac{\partial f}{\partial t}\, dA + \int_{\partial A} f V_n\, ds)$$

J^d cannot be reduced to a line integral, though it is not dependent on the contour, as follows from (12) and σ_{ij} and n_1 vanishing on the crack edges.
Consider a rectangular contour $x_1'=\pm a$, $x_2'=\pm\eta$ around the crack in a coordinate system OX_1', X_2' moving along with the crack with constant length 2a and velocity V (OX_1' is along the crack). As $\rho u_i, t u_i, 1 n_1$ integrated over a vanishing circle around the crack tip is zero {Afanasev and Cherepanov (17)}, A can be replaced by Γ and the surface integral term for J^d vanishes for this contour flattened on the crack and J^d reduces to (15):

$$J^d = \int_{-a}^{a} -2\sigma_{22}(x_1',\eta)u_{2,x_1'}(x_1',\eta)dx_1', \quad \ldots\ldots(13)$$

Using the asymptotic solutions for $\sigma_{22}(x_1',x_2')$ and $u_2(x_1',x_2')$ for the stationary state, Sih {(18), (14)}, one finds for plane strain and opening mode I, cf. (15):

$$J^d = \frac{1-\nu^2}{E} K_I^{\sigma} K_I^{u} \quad \ldots\ldots(14a)$$

which proves equal to the energy flux G in that case as well (15). Also for the arbitrary transient case, as was demonstrated by Achenbach and Bazant (19) and also by Bui (15).

$$J_I^d(t) = \frac{1-\nu^2}{E} K_I^{\sigma}(t) K_I^{u}(t) \quad \ldots\ldots(14b)$$

The evaluation of J^d from (12) obviously poses difficult experimental problems. Apparently (14b) offers perspectives from measurements of $K_I^{\sigma}(t)$ and V, as:

$$J_1^d(t) = \frac{1-\nu^2}{E}\{K_1^{\sigma}(t)\}^2 \frac{4}{\kappa+1} f(V);\ f(V) = \frac{\alpha_d(1-\alpha_s^2)}{4\alpha_s\alpha_d-(1+\alpha_s^2)^2} \quad \ldots(14c)$$

$$f(V) = \frac{c_d^2}{2c_d^2-2c_s^2} + \alpha V^2 + \ldots = \frac{\Lambda+2\mu}{2(\Lambda+\mu)} + \alpha V^2 + \ldots \text{ for } V \ll c_R$$

For α was found: $\alpha = \dfrac{3c_d^4 - 4c_d^2c_s^2 + 3c_s^4}{8c_s^2(c_d^2 - c_s^2)^2} = \dfrac{(\Lambda+2\mu)3\Lambda+\mu)+3\mu^2}{8\mu(\Lambda+\mu)^2}\rho$

N.B: 1° $\lim\limits_{V\to o} f(V) = \dfrac{c_d^2}{2c_d^2 - 2c_s^2} = \dfrac{\Lambda+2\mu}{2(\Lambda+\mu)}$ and as required by (14b)

for plane strain: $\dfrac{4}{\kappa+1}\ \dfrac{\Lambda+2\mu}{2(\Lambda+\mu)} = 1$

and for plane stress: $\dfrac{4}{\kappa+1}\ \dfrac{\Lambda+2\mu}{2(\Lambda+\mu)} = \dfrac{1}{1-\nu^2}$

2° for $\nu=\frac{1}{4}$ is $\Lambda=\mu$ and $\lim\limits_{V\to 0} f(V) = \frac{3}{4}$ and $\alpha=\frac{9}{16}\frac{\rho}{\mu}$

3° for $V=c_R$ is $4\alpha_s\alpha_d - (1+\alpha_s^2)^2 = 0$ and $f(V) \to \infty$

As $K_I^{\sigma}(t) = 3(2\pi)^{\frac{1}{2}}\mu\ Q\ \dfrac{4\alpha_s\alpha_a - (1+\alpha_s^2)^2}{4(1+\alpha_s^2)}$ {Rice (20)}

with Q a parameter with dimensions $[m^{\frac{1}{2}}]$ determined by the boundary conditions, one has from (14c):

$$J_1^d(t) = \frac{1-\nu^2}{E}\ \frac{9\pi\mu^2}{\kappa+1}\ Q^2\ \frac{\alpha_d\ (1-\alpha_s^2)\quad \{4_s\alpha\ \alpha_d-(1+\alpha_s^2)^2\}}{2\ (1+\alpha_s^2)^2} \qquad (14d)$$

From (10b) one alternatively concludes:

$$J_I^d(t) = \frac{1-\nu^2}{E}\ K_I^2\ \left(\frac{1-\beta}{1+\beta}\right)^{\frac{1}{2}}; \qquad \ldots\ldots\ldots\ldots\ldots\ldots\ldots\ldots\ldots\ldots (14e)$$

for $V \ll c_R$, $J^d(t) \cong \frac{1-\nu^2}{E}\ K_I^2(1-\beta^2)^{\frac{1}{2}}$

Both (14d) and (14e) imply: for $V\to c_R$, $J_I^d(t)\to 0$ and for $V\to 0$, $J_I^d(t)\to J_I$. For $t = t_a$ at arrest $J_I^d(t_a) = J_{I\,a}^d(V)$ presents itself as arrest characterising material feature, with V just before arrest, after which V (usually) shows a (sudden) drop to zero at arrest. As V here remained rather constant $J_{I\,a}^d(V)(:)(K_{1\,a}^s)^2$. K_1^s is evaluated using stress recordings of straingauges localised near the path of the extending crack - and not according to here unadequate stress calculations based on quasi static compliance changes, in view of stresswaves reflected. V-evaluations are also provided by the straingauges responses.
(14d) rather combines the conclusion of Broberg (21): $G^d = (1-V^2/c_m^2)G^s$ with $c_m = 0.38\sqrt{E/\rho} \sim 0.69\ c_R$ and that of (11), Glennie (22) or the earlier given analysis here (6d), the latter being based on surface observations.

Usually the finite dimensions of specimens or structural parts will imply that stress waves reflected from their sides will add to tension stress at the crack tip, favoring propagation as stated before. This means that kinetic energy is used again for driving the crack as at the base of the BCL-considerations. Before such a reflected stress wave reaches the crack tip $G_1^d \{=G_1^\sigma(t)\}$ will be below $G_1^s(t)$. Thereafter with periodical fluctuations corresponding with the reflection frequency, as dictated by dimensions, it can remain above G^s and provide for arrest if G_1^d sinks below the fracture toughness at the relevant strain rate. In the arrested situation G_1^d will damp out to G_1^s; cf. Kalthoff et al. (23), who also propose a (RDE=) "reduced dynamic effect" specimen in which the geometrical shape provides for a strong suppressing of stress waves reflection (24).

CONCLUSIONS

The BCL and MRL procedures for assessment of an arrest characterizing s.i.f., require still several corrections as indicated. Testing a steel of practical interest, like Fe510, according to these procedures encounters severe difficulties a.o. in view of the unavoidable introduction of internal stresses at specimen preparation.

Reflection of stress waves at unstable crack extension can lead to large discrepancies between static and dynamic s.i.f. determinations at arrest. If on the other hand those reflections are negligeable BLC- and MRL-methods lead to rather similar results.

Dynamic evaluation of the s.i.f. at arrest, using photostress and (or) straingauges techniques with Robertson test plates, presumably showing pronounced stress waves reflections, compares to BCL (and MRL) estimates from CWCL-specimens at lower test temperature, assuming a relevant temperature dependence of the s.i.f. at arrest.

An experimental method, which both accounts for possible stress waves reflections and takes care of "pure" dynamic effects (as occurring in a plate with infinite dimensions) is the observation of the response of straingauges near the crackpath, allowing the necessary stress and fracture velocity estimates.
Besides a "dynamic" s.i.f. this allows the indication of a preferable "dynamic" J at arrest.

ACKNOWLEDGEMENTS

This contribution was based on work performed under convention 7210-KE/602 of the European Community for Carbon and Steel with Metal Research Institute TNO, Apeldoorn, The Netherlands. The experimental work was performed with assistance of Messrs. M.A. Lont and J. Nieuwpoort, while Messrs. H. Wildschut and F.H. Toneman contributed to analytical and numerical aspects resp.

REFERENCES

(1) Prospective for a cooperative test program on crack arrest toughness measurement (to be conducted under the auspices of ASTM E 24-03-04.)
Subcommittee on dynamic testing, dynamic initiation, (crack arrest task group - program coordinator G.T. Hahn)

(2) In ASTM-STP 627. "Fast Fracture and Crack Arrest" (editors: Hahn, Kanninen; Chicago 1976)
  (a) Kanninen, M.F.; Popelar, C. and Gehlen, P.C. - Dynamic analysis of crack propagation and - arrest in double cantilever beam specimen.
  (b) Hoagland, P.G.; Rosenfield, A.R., Gehlen, P.C. and Hahn G.T. - A crack arrest measuring procedure for K_{Im}, K_{Id} and K_{Ia} properties.
  (c) Crosley, P.B. and Ripling, E.J. - Towards development of a standard test for measuring K_{Ia}.

(3) Kanninen, M.F. - Int.Journal of Fracture 10, 1974, pp.45

(4) In ASTM-STP711 "Crack arrest methodology and applications" (editors: Hahn, Kanninen; Philadelphia, 1978)
  (a) Crosley, P.B. and Ripling, E.J. - Comparison of crack arrest methodologies
  (b) Hahn, G.T.; Hoagland, R.G.; Rosenfield, A.R. and Barnes, C.R. - A cooperative program for evaluating crack arrest testing methods

(5) Tada, H., Paris, P. and Irwin, G.R. "The stress analysis of Cracks Handbook" - Del Research Corp. (Saint Louis, 1973)

(6) Newman, J.C. - NASA TN D-8269, July 1976

(7) Roberts, E.Jr. - Materials Research and Standards, vol.9, 1969, p.27

(8) Elst, H.C. van; Wildschut, H.; Lont, M.A. and Toneman, F.H. - Mechanical parameters and material properties conditioning arrest of unstable cracks. Final Report 83M/42/0772 of Metal Research Institute TNO to ECSC-Convention 7210-KE/602

(9) Rossmanith, H.P. and Irwin, G.R. - Analysis of dynamic isochromatic stress pattern - Report of the Dept. of Mech.Eng., Glenn L. Martin Institute of Technology, University of Maryland, USA, 1980

(10) Kanazawa, T.,; Machida, S.; Yajima, H. and Kawano, H. -IIW-Document No. X-984-81

(11) Freund, J. - Journal of Mechanics and Physics of Solids 20, 1972, pp. 141-152

(12) In ASTM-STP514 "Fracture Toughness". University of Illinois, Urbana-Champaign, Ill. 1971
Sailors, R.H. and Corten, H.T. - Relationship between material fracture toughness using fracture mechanics and transition temperature tests

(13) Benthem, J.C. and Koiter, W.L. - Asymptotic approximation to crack problems. In: "Mechanics of Fracture" Vol. 1 Methods of analysis and solution of crack problems (Ed. G.C. Sih at Noordhoff Int.Publ.C^{V}. Leyden, 1973)

(14) Bui, H.D. - Proc.ICF$_4$ Waterloo, Canada, 1977, vol. 3, p. 91

(15) Bui, H.D. - "Mécanique de la rupture fragile" (Published by Masson, Paris 1978)

(16) Fletcher, D.C. Arch.Rat.Mech.Anal. 60, 4, 1976, p.329

(17) Afanasev, E.E. and Cherepanov, G. - PMM 37, 4, 1973, p. 618

(18) Sih, G.C. "Handbook of stress intensity factors" (Lehigh University, Bethlehem 1973)

(19) Achenbach, J.D. and Bazant, L.P. - Journ. of Appl. Mech. 42, 1975, p. 183

(20) In "Fracture", ed. by H. Liebowitz at Academic Press (1968), Vol II, Ch. 3; p. 236.
Rice, J.R. - Mathematical analysis in the mechanics of fracture; p. 191.

(21) Broberg, K.B. - in Recent Progress in Applied Mechanics, (Almquist and Wicksell, Stockholm, 1967) p. 125

(22) Glennie, E.B. and Willis, J.R. - Journal of Mechanics and Physics of Solids, 19, 1970, p. 11

(23) In ASTM STP611 "Crack Arrest Methodology and Applications", Philadelphia, Pa, USA, 1980
Kalthoff, J.F.; Beinert, J.; Winkler, G.; Klemm, W. - Experimental analysis of dynamic effects in different crack arrest test specimens, p. 109

(24) Kalthoff, J.F.; Beinert, J.; Klemm, W.
Mechanik und Stoffverhalten bei der Arretierung von Rissen. Final report of Fraunhofer Institute for Materials Mechanics to ECSC-Convention 7210-KE/107, 1984

NOMENCLATURE

Symbol:	Means:	Dimensions:
K	s.i.f.	$(MNm^{-3/2})$
G	c.d.f.	(MNm^{-1})
J	p.i.i.	(MNm^{-1})
Y,χ,H	geometrical correction function	
σ	stress	(MNm^{-2})

E	Young's modulus	(MNm^{-2})
μ	shear modulus	(MNm^{-2})
ν	Poisson's ratio	
Λ	Lamé constant	
V	fracture velocity	(ms^{-1})
c	sound wave velocity	(ms^{-1})
Δ	displacement of crack edges at specified distance from loadline	(m)
v	displacement of crack edges in loadline	(m)
θ	polar angle w.r.t. crack tip	
r	polar radius w.r.t. crack tip	(m)
p	distance to crack path	(m)
β	V/c_R	
L	length	(m)
W	width	(m)
a	crack length	(m)
λ	a/W	
ω	W/L	
B	thickness	(m)
P	load	(kN)
C	compliance	(mN^{-1})
k	1 in plane stress $1-\nu^2$ in plane strain	
κ	(3-ν)/(1+ν) in plane stress 3-4ν in plane strain	
n	normal or integer	
u	displacement	(m)
w	elastic strain energy density	(MNm^{-2})
A	surface	(m^2)
s	path	(m)
t	time	(s)

Subscript:	to:	Means:
I,II,III	K,G,J	fracture mode
c	K,G,J	critical
m	K,G,J	at arrest
a	K,G,J	"static" arrest
d	K,G,J	"dynamic" arrest
Q	K	initiation
i	Δ,v,Y,χ	at initiation
a	a,Δ,v,Y,χ,t	at arrest
R	c	Rayleigh
d	c	dilatational
s	c	shear

o	a,r,C,ε,σ,P	initial
x,y,z	σ,ε,u	cartesian coordinates
i,j,k	σ,ε,u	" "
Y	σ	yield stress
M	C	machine
N	B	side grooved

Superscript:	to:	Means:
d	K,G,J	dynamic
s	K,G,J	static
σ	K,G,J	dynamic
u	K,G,J	kinematic
**	G	$G/E\varepsilon_o^2 W$
*(*)	K	corrected

Abbreviations:

ASTM	=	American Society for Testing Materials
BCL	=	Battelle Columbus Laboratories, Ohio, USA
MRL	=	Materials Research Laboratories, Illinois, USA
ARRAP	=	ASTM Round Robin Arrest Program
s.i.f.	=	stress intensity factor
c.d.f.	=	crack driving force
p.i.i.	=	path independent integral
RCAT	=	Robertson test crack arrest temperature
CLWL	=	crack line wedge loaded
SENT	=	single edge notch tensile
CNT	=	central notch tensile
SENB	=	single edge notch bend
CT	=	compact tension
h.s.p.	=	high speed photography
UTS	=	ultimate tensile strength

Keywords:
Critical fracture toughness at arrest; high speed photography; dynamic isochromatics; straingauges recordings; dynamic stress intensity factor, crack driving force, J-integral; quasi static crack extension; fixed rigid edges displacement; arrest temperature; stress relaxation; stress waves reflection.

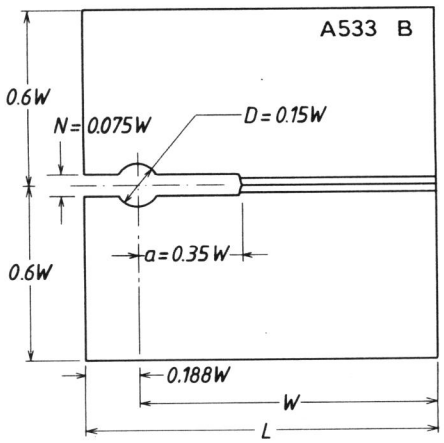

Fig.1a CLWL-MRL weld embrittled crack arrest specimen W=169.4 mm; D=25.4 mm; B=50.8 mm; a= 59 mm; N=12.7 mm; B_N= 0.75 B

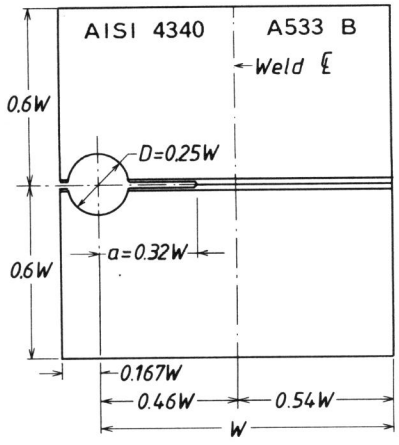

Fig.1b CLWL-BCL duplex crack arrest specimen W=208 mm; D=52 mm; B=50.8 mm; a=66.6 mm; B_N= 0.75 B

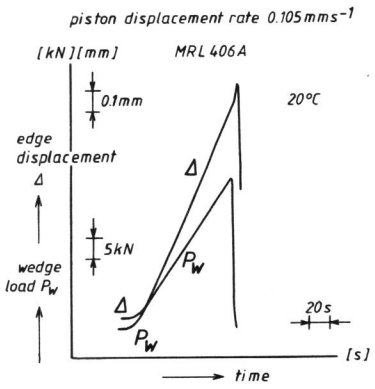

Fig.2a Wedge load and notch opening displacement reading at CLWL-MRL specimen testing.

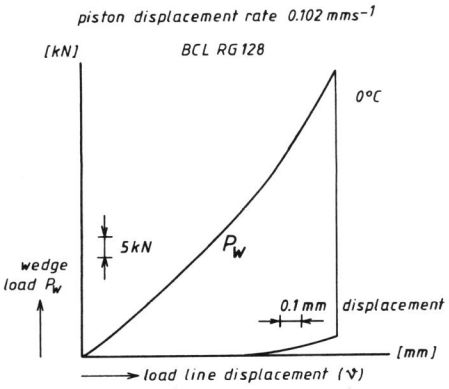

Fig.2b Wedge load vs. loadline displacement at CLWL-BCL specimen testing.

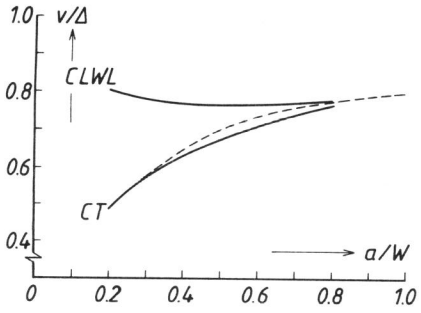

Fig.3 v/Δ vs. λ=a/W for CLWL- and CT-specimen. Full line: results according to Newman (6); dashed line: data used by Crosley and Ripling (3), (7).

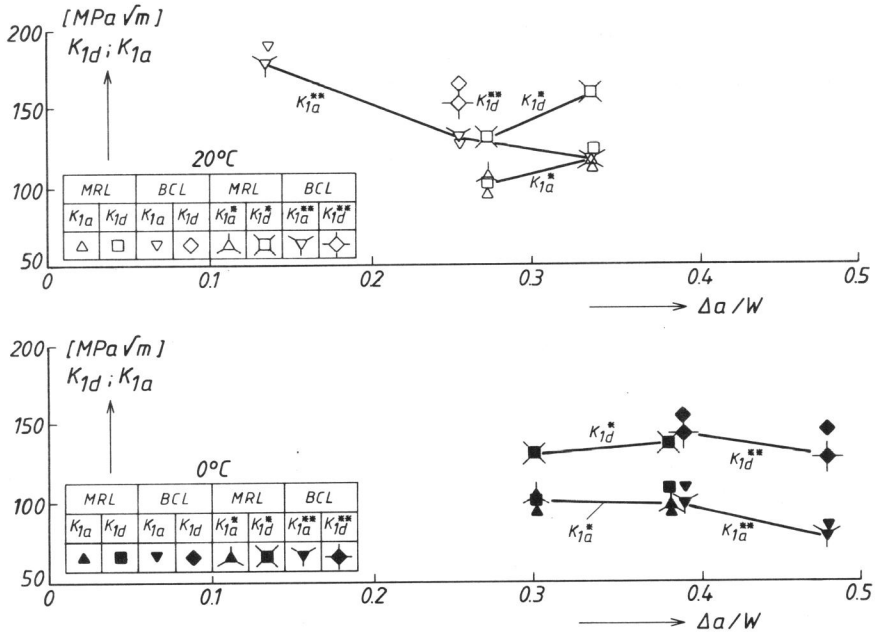

Fig.4 Uncorrected and corrected K_{Id} and K_{Ia} results in ARRAP for MRL and BCL testing procedure at 20°C and 0°C resp. for some crackjumps.

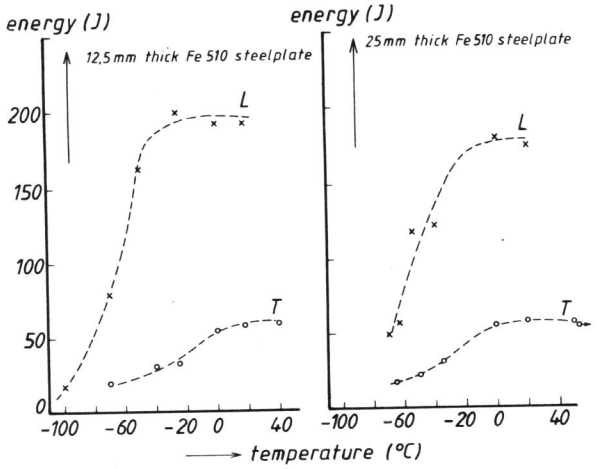

Fig.5a Charpy-V curve for longitudinal and transversal testing of 12.5 mm thick Fe510 steel plate.

Fig.5b Charpy-V curve for longitudinal and transversal testing of 25 mm thick Fe510 steel plate.

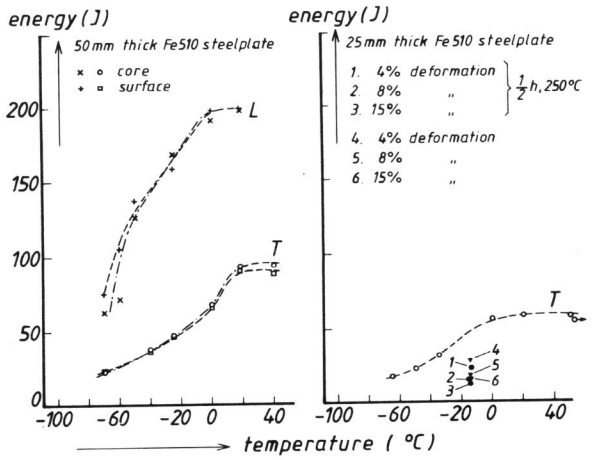

Fig.5c Charpy-V curve for longitudinal and transversal testing of 50 mm thick Fe510 steel plate (core and surface).

Fig.5d Charpy-V results for transversal testing of deformed and aged 25 mm thick Fe510 steel plate.

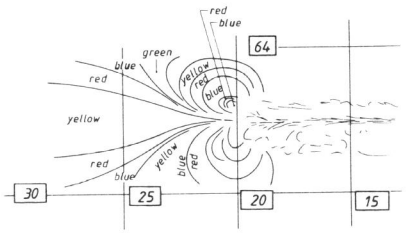

Fig.6 Isochromatics in 1 mm thick photo-elastic layer PS-8c glued to a 25 mm thick Robertson test Fe510 steel plate (length x width = 1000 mm x 300 mm) with arresting crack at -10°C. (drawn after h.s.p. colour recording with 207.000 f/s.)

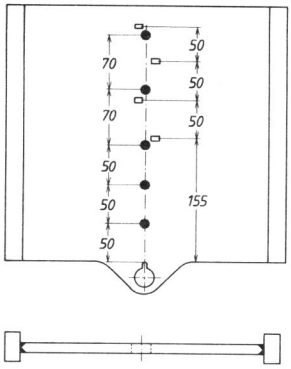

Fig.7a Straingauges instrumented Robertson test specimens for 12.5 and 25 mm thick Fe510 steel plate.

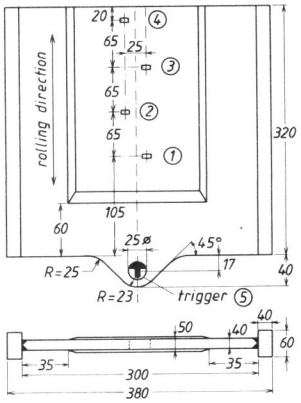

Fig.7b Straingauges instrumented Robertson test specimens for 50 mm thick Fe510 steel plate.

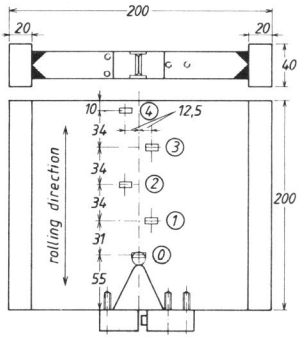

Fig.8 Straingauges instrumented SENT-test specimens for 12.5 and 25 mm thick Fe510 steel plate.

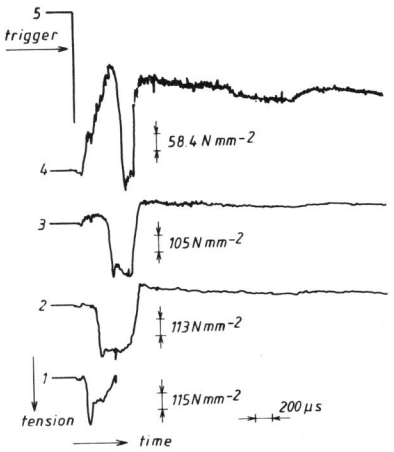

Fig.9a Straingauges recordings of just passing through crack in 50 mm thick Fe510 steel plate Robertson test specimen no. 22 at -10°C.

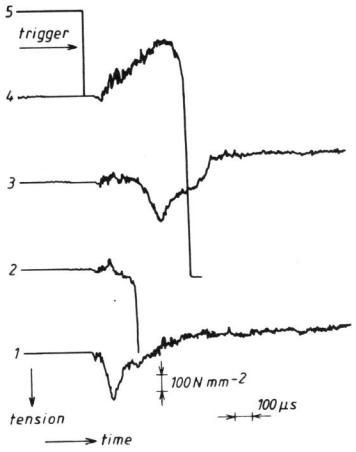

Fig.9b Straingauges recordings of just passing through crack in 50 mm thick Fe510 steel plate Robertson test specimen no. 23 at -5°C.

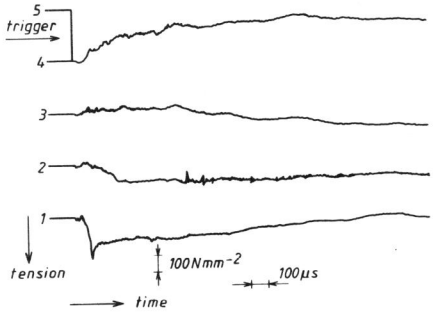

Fig.9c Straingauges recordings of arresting crack in 50 mm thick Fe510 steel plate Robertson test specimen no. 24 at 0°C.

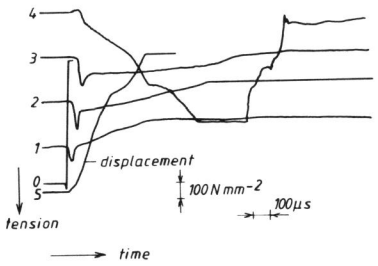

Fig.9d Straingauges recordings of arresting crack in 25 mm thick Fe510 steel plate SENT-specimen no. 25 at -19°C.

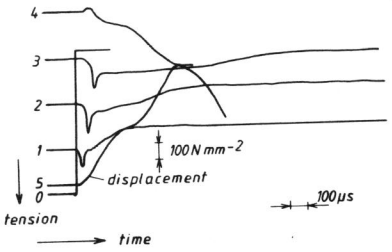

Fig.9e Straingauges recordings of arresting crack in 25 mm thick Fe510 steel plate SENT-specimen no. 29 at -19°C.

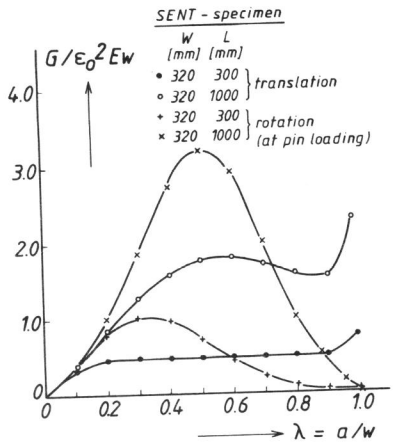

Fig.10a Dimensionless c.d.f. at quasi static crack extension for fixed rigid edges displacement in SENT-specimen.

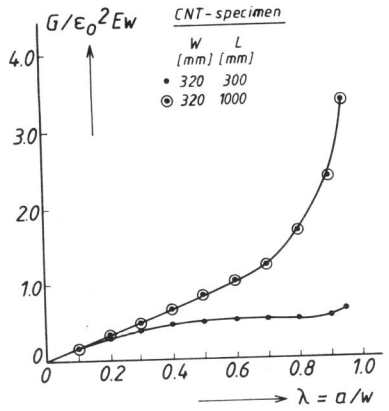

Fig.10b Dimensionless c.d.f. at quasi static crack extension for fixed rigid edges displacement in CNT-specimen.

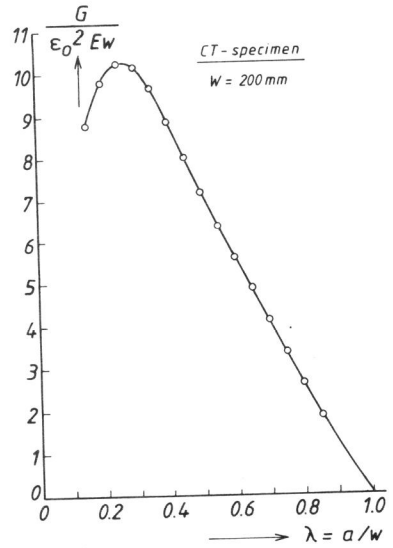

Fig.10c Dimensionless c.d.f. at quasi static crack extension for fixed rigid edges displacement in CT-specimen.

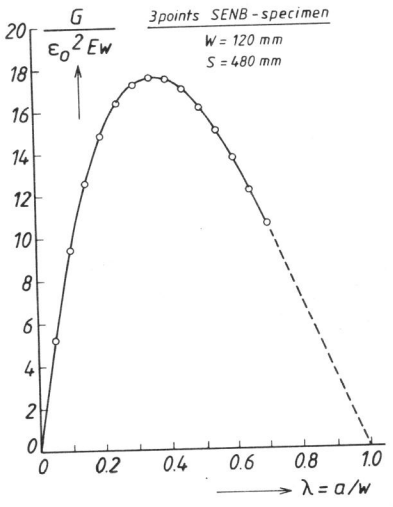

Fig.10d Dimensionless c.d.f. at quasi static crack extension for fixed rigid edges displacement in 3 points SENB-specimen.